Collision-Energy-Resolved Penning Ionization Electron Spectroscopy of Glycine with He(2^3S) Metastable Atoms: Conformational Isomers in Collisional Ionization

Yoshihiro Yamakita* and Koichi Ohno

Department of Chemistry, Graduate School of Science, Tohoku University, Aramaki, Aoba-ku, Sendai 980-8578, Japan

Received: April 28, 2009; Revised Manuscript Received: July 7, 2009

Conformationally dependent ionization of the simplest amino acid, glycine, is studied by Penning ionization electron spectroscopy with velocity-resolved metastable He*(2^3S) atoms. The observed He I ultraviolet photoelectron and Penning ionization electron spectra are reproduced by superimposed theoretical spectra, assuming thermal distributions of conformers. The conformations of amino acids are determined by analyzing the observed Penning ionization cross sections, peak shifts, and collision energy dependences of partial ionization cross sections (CEDPICS). The Penning ionization cross sections are governed by collisionally accessible exterior electron densities. When the amino and carbonyl groups are exposed to He* access, the nonbonding orbitals of N (n_N) and O atoms (n_O) give rise to strong bands. The observed negative peak shifts and negative CEDPICS for the n_N and n_O orbitals suggest the presence of attractive interactions around their electron distributions. The most attractive wells are estimated to be ~400 meV in the direction of the n_N orbitals by ab initio model calculations. A conformer possessing dual hydrogen bonds contributes predominantly to the spectra.

1. Introduction

Amino acids, which possess NH_2 and COOH groups, are known to be conformationally flexible. The simplest amino acid, glycine, has three rotational degrees of freedom on C−C, C−N, and C−O bonds (see Figure 1). It exists in nonzwitterionic states in the gas phase.[1] The flexibility around these single bonds gives rise to conformational isomers, such as those in Figure 1. The conformational stability is affected by competitive forces between attractive hydrogen-bonding and repulsive eclipsed single-bond interactions. As a result, the potential energy surface (PES) displays many local minima separated by conformational barriers. Because the potential energy landscape will ultimately determine the structures of the proteins, the electronic property of amino acids is an important subject for study.

There have been extensive experimental studies on glycine. In particular, structural determinations have been performed by microwave or millimeter-wave spectroscopy[2−8] and electron diffraction experiments.[9] Infrared spectroscopy has been applied to glycine conformers in rare-gas matrixes[10,11] and helium droplets.[12] Theoretical calculations have also been performed on the simplest amino acid as a benchmark system. Five to eight conformers have been predicted by ab initio self-consistent-field (SCF) calculations at the early stage,[13,14] and the importance of electron correlation effects has been realized.[15−24] To date, a number of quantum chemical calculations have been performed at correlated levels using extended basis sets. These include Møller−Plesset perturbation theory[8,11,15,16,19,23,24] calculations up to the fourth order (MP4),[17] configuration interaction calculations including single and double excitations (CISD),[18] coupled cluster calculations with single, double, and perturbative triple excitations [CCSD(T)],[17,18] and density functional theory (DFT) calculations.[25]

The conformational isomers exist in a close energy range on the order of 1−10 kJ mol^{-1} (Figure 1),[17] and conformational energy barriers are significantly small, within ~3 kJ mol^{-1}. Such a shallow PES leads to conformational dynamics at a finite temperature[7] and plays a fundamental role in real biological systems. Spatial distributions of the nonbonding orbitals of heteroatoms are connected with hydrogen bonding, and their electronic distributions are modulated on the course of large-amplitude motion. Also, zwitterionic forms and proton-accepting/donating reactions are involved in aqueous media. Quantum chemical studies on these electronic properties can form foundations for research on biological functions or drug designs.

Photoionization of glycine has been recorded by He I and He II ultraviolet photoelectron spectroscopy (UPS) experiments,[26−29] and the electronic wave functions have been

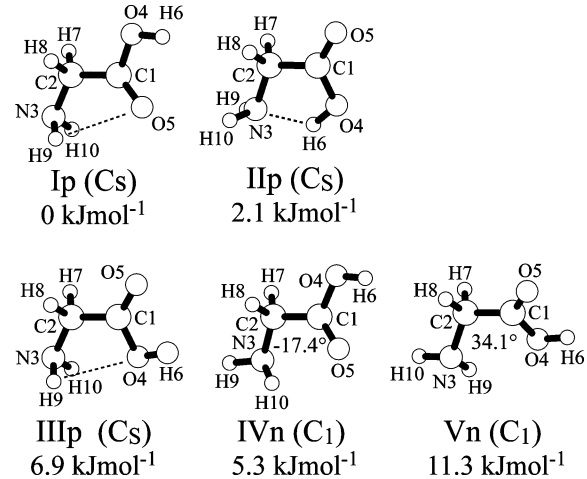

Figure 1. Conformational isomers of glycine. Relative electronic energies ΔU calculated at the B3LYP/aug-cc-pVTZ level of theory are given. Conformers II and III with the C_s point group correspond to average structures along torsional modes about the CC bonds because twisted structures are calculated to be equilibrium structures slightly below ΔU (see Table 1).

* E-mail: yy@qpcrkk.chem.tohoku.ac.jp.

10.1021/jp9038978 CCC: $40.75
Published on Web 09/11/2009

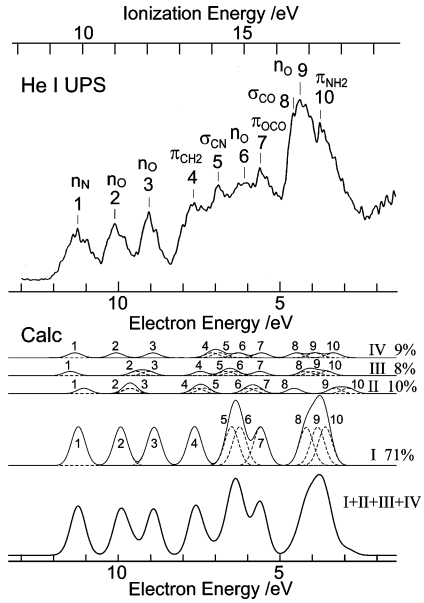

Figure 2. He I UPS spectrum of glycine (260 °C) in comparison with the theoretical spectra of glycine conformers I−IV. The positions of the bands are those obtained from OVGF calculations, and partial cross sections are proportional to the pole strengths. The bands have been convoluted by Gaussian bandwidths (fwhm = 0.5 eV).

determined by electron-impact, electron momentum spectroscopy (EMS) experiments.[20,22] The observed bands have been assigned to Dyson orbitals by performing electron propagator calculations,[24,25] and the momentum profiles have been well reproduced by the DFT calculations.[20,22,25] However, the flexible conformations make the spectra complicated under thermal conditions, where the observed UPS and EMS are essentially convoluted by thermal distributions. Thus, assignments for ionizations from deep molecular orbitals (MOs) 17-11 have remained unestablished, and experimental approaches of other kinds have been desired.

Penning ionization[30] is an elementary process that takes place upon collision between a molecule and a metastable atom.[31] The metastable atom A* with an excitation energy exceeding the lowest ionization energy (IE) of the molecule M leads to ionization of M along with deexcitation of A*:

$$A^* + M \rightarrow A + M_i^+ + e^- \qquad (1)$$

This process proceeds in the electron-exchange mechanism as proposed by Hotop and Niehaus.[32] Electron 1 transfer from a MO ϕ_i of M into the inner vacant orbital χ of A* and electron ejection from the outermost orbital χ' of A* to the continua ϵ take place simultaneously. Thus, the interaction of particles gives rise to unique properties. Those include preferential ionization from exposed functional groups and collision-energy-dependent ionization dynamics. The cross section depends upon collisional dynamics in the region where ϕ_i extends. The selectivity of the outermost electron distributions would be enhanced when any part of the molecule is exposed to or encapsulated from the He* access. In this sense, the higher structures of flexible molecules or surface structures of condensed molecules are expected to display much stronger steric preferences compared to those of photoionization. Thus, the collisional ionizations of simple biomolecules are of interest as experimental and theoretical benchmark systems.

In this paper, we report on collision-energy-resolved Penning ionization electron spectroscopy (PIES) spectra of glycine as the first example of amino acids. The conformational dependence of ionization is discussed on local interaction potentials with He*(2^3S). Outer-valence Green's function (OVGF) calculations and ab initio model potentials between conformers and He* are calculated extensively with correlation-consistent, extended basis sets. Band assignments are fully established based on the experimental PIES and collision energy dependences of partial ionization cross sections (CEDPICS). This benchmark system exemplifies the applicability of PIES to thermally fluctuating, hydrogen-bonded systems. The present approach can be extended to larger biochemical species including proteins and hydrogen-bonded clusters. Experimental difficulties from a low number density can, in principle, be overcome by using a highly sensitive electron spectrometer.[33] Such efforts could lead to extensive studies of various biomolecules using collisional electron spectroscopy.

2. Experimental Section

2.1. Electron Spectroscopy. A portion of glycine powder was placed in an aluminum container with 8 mm inner diameter and 16 mm length, which was attached to the collision cell. The container was carefully heated to ~260 °C with a ceramic heater so that the vaporized samples did not quench a metastable atom beam too much. The effusive vaporization without high stagnation pressures is expected to give statistical thermal distributions at the temperature maintained. That is, collisional effects such as supersonic cooling and collision-induced conformational rearrangements need not be considered here. The temperature was monitored by a chromel−alumel thermocouple. The density of the sample molecules was monitored by a vacuum gauge and a Faraday cup at a terminal position of the beam. The stability of the sample pressure is crucial for collision-energy-resolved measurements. The thermal conduction from the container to the collision cell prevents sample deposition on the inner wall. The samples were purchased from a commercial source and used without further purification.

TABLE 1: Relative Energies (kJ mol^{-1}) of Glycine Conformers

	B3LYP/aug-cc-pVTZ		MP2/aug-cc-pVTZ				
conformer	ΔU	ΔU_{ZPT}[a]	ΔU	ΔU_{ZPT}[a]	B3LYP/aug-cc-pVDZ[d]	MP2/6-311++G(d,p)[e]	expt
Ip	0.00	0.00	0.00	0.00	0.00	0.00	
IIp	2.10	2.95	1.76	3.10		2.46	6.7,[f] 8.4[g]
IIn	2.07	3.40	1.51	3.43	2.40	2.21	
IIIp	6.86	6.97	7.00	7.44		6.66	3.8[f]
IIIn	6.84[b]	6.77[b]	7.00[c]	7.26[c]	6.86	6.03	
IVn	5.31	5.00	4.86	5.06		5.29	
Vn	11.32	11.23	10.69	11.27		9.2	

[a] ZPEs calculated at the B3LYP/aug-cc-pVTZ level are included. [b] Dihedral angle ϕ_{4123} is 2.96°. [c] Dihedral angle ϕ_{4123} is −0.02°. [d] ΔU in ref 11. [e] ΔU in ref 24. [f] Matrix-isolation infrared spectroscopy in Ne.[10] [g] Microwave spectroscopy.[8]

TABLE 2: Comparisons of Observed and Calculated IEs (eV), Observed Slopes (*m*), Assignments, and Exterior Electron Densities (EEDs) of Glycine Conformer I

	IE						OVGF			
band	He I[a]	He II[b]	PIES[c]	ΔE/eV[d]	M[e]	MO	cc-pVTZ[f]	TZVP[g]	P3 6-311G(d,p)[i]	EED[j] (%)
1	9.9	10.0	10.2	−0.33	−0.42	16a′ (n_N)	9.98(0.91)	10.0	9.9	4.38
2	11.0	11.1	11.1	−0.11	−0.27	15a′ ($n_{O_{\parallel}}$)	11.29(0.91)	11.4	11.0	2.50*
3	12.1	12.2	12.1	0.0	−0.30	4a″ ($n_{O_{\perp}}$)	12.33(0.90)	12.4	12.2	2.93*
4	13.4	13.6			–0.24	3a″ (π_{CH_2})	13.58(0.92)	13.6	13.5	2.47
5	14.2	14.4	14.6	−0.4	−0.31	14a′ (σ_{CN})	14.72(0.91)	14.8	14.6	2.38
6	15.0	15.0	(15.3)	(−0.3)	−0.32	13a′ ($n_{O_{\parallel}}$)	14.97(0.91)	15.1	14.8	1.74
7	15.5	15.6	(15.6)	(−0.1)	−0.35	2a″ (π_{OCO})	15.62(0.90)	15.8		2.55
8	16.5	16.6			−0.28	12a′ (σ_{CO})	17.03(0.90)	17.7[h]		1.55
9	16.7	16.9	(17.0)		−0.31	11a′ ($n_{O_{\parallel}}$)	17.38(0.91)	17.2[h]		1.51
10	17.4	17.6				1a″ (π_{NH_2})	17.62(0.91)	17.7		2.84

[a] He I photoelectron spectroscopy (this work). [b] He II photoelectron spectroscopy.[28] [c] Nominal values corresponding to the IE are given. [d] Peak shifts from the corresponding UPS bands for PIES bands. [e] Slope parameters obtained from linear regression analyses for collision energy dependences shown in Figure 4. [f] This work. Pole strengths are in parentheses. [g] Reference 25. [h] The orders of these IEs are reversed compared to this work. [i] Reference 24. [j] EEDs calculated at the SCF/6-311++G(d,p) level of theory. Asterisks indicate those involved in hydrogen bonding.

The experimental apparatus has been reported previously.[34,35] Briefly, electron energy spectra upon collisional ionization were recorded with a hemispherical electrostatic, deflection-type analyzer. The electron collection angle was set as 90° to an incident He*(2^3S) beam. A metastable He*(2^3S) beam having excitation energy 19.82 eV was prepared by direct-current discharge. He*(2^1S) components were radiatively quenched by a water-cooled He discharge lamp, and ionic and excited He species were removed by an electric deflector. The transmission efficiency curve for the electron-energy analyzer was calibrated by comparing the recorded He I UPS of standard samples and those of Gardner and Samson[36] and Kimura et al.[37] The resolution of electron energy was estimated to be ~70 meV from full width at half-maxima (fwhm) of the $Ar^+(^2P_{3/2})$ photoionization peak.

2.2. Collision Energy. Collision-energy-resolved measurements were performed under an electron energy resolution of ~250 meV by applying the cross-correlation time-of-flight (TOF) technique to the He* atom beam with a mechanical chopper of the pseudorandom type over a flight length 504 mm.[38] The relative velocity v_r gives the collision energy E_c as

$$E_c = \frac{1}{2}\mu v_r^2 \tag{2}$$

$$v_r = \sqrt{v_{He^*}^2 + \frac{3k_BT}{m}} \tag{3}$$

where k_B is Boltzmann's constant, m is the mass of the target molecule, μ is the reduced mass of the colliding system, and T is the temperature of the sample. The TOF distribution of the thermal He* beam is determined by counting the secondary electrons from a stainless steel plate in the collision cell. The fact that the TOF of the electrons is negligibly short compared to that of the He* atoms allows us to evaluate the velocity distribution of He*(v_{He^*}) from the electron signals. Partial ionization cross sections $\sigma^{(i)}(E_c)$ are obtained by normalizing the electron signals from the sample to the distribution as a function of the collision energy.

3. Calculations

3.1. Quantum Chemical Calculations. Structural parameters were optimized by ab initio and DFT calculations at the MP2 and B3LYP[39,40] levels, respectively. The intramolecular potential involving long-range interactions of nonbonding orbitals was evaluated using augmented correlation-consistent, polarized valence triple-ζ (aug-cc-pVTZ) (6D, 10F) basis functions.[41,42] The adiabatic IEs were obtained from OVGF calculations using cc-pVTZ functions. These quantum chemical calculations were performed with the *Gaussian 03* program[43] on the parallel computing server (Fujitsu Primequest) at the Research Center for Computational Science of the National Institutes of Natural Science or in-house dual Xeon computers.

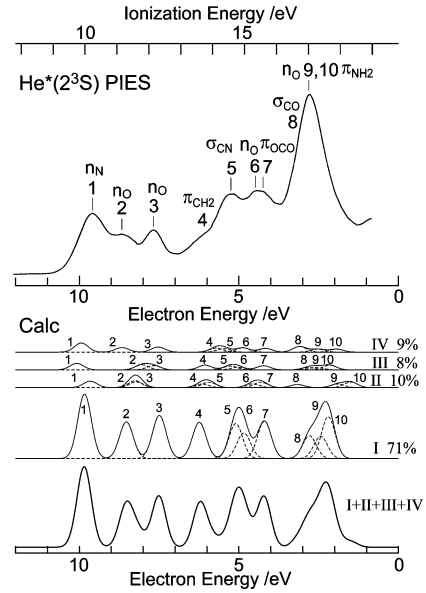

Figure 3. PIES spectrum of glycine (260 °C) with He*(2^3S) in comparison with theoretical spectra of glycine conformers I−IV. The positions of bands are those obtained from OVGF calculations, and partial cross sections are proportional to EEDs. The bands have been convoluted by Gaussian bandwidths (fwhm = 0.5 eV).

3.2. Penning Ionization Cross Sections. As mentioned in section 1, partial ionization cross sections for Penning ionization are governed by overlap between molecular and atomic orbitals upon collision due to the electron-transfer mechanism.[32] The amount of orbital overlap can be estimated approximately using the exterior electron density (EED) model.[44,45] The EED is defined by

$$(\mathrm{EED})_i = \int_\Omega |\phi_i|^2 \, d\tau \quad (5)$$

where Ω is the area where He* is accessible or simply outside repulsive surfaces. As a first approximation, we used the van der Waals (vdW) sphere[46] in the definition of Ω. This simple model allows us to compare the PIES cross sections for different isomers on the same basis, and collisional dynamics can be investigated independently. The EEDs were obtained from numerical integration employing grid points at 0.1 Å intervals for each SCF MO ϕ_i on the basis of 6-311++G(d,p) (6D). The 6-311++G(d,p) basis functions have been reported to give satisfactory electron momentum profiles.[22] The combination of OVGF and EED calculations have well reproduced PIES of other molecules.[47] The robustness of the EED approximation is supported by the asymptotic behaviors of MOs around the vdW surfaces. As a general trend, the logarithms of the EED values change monotonically, and approximately linearly, in proportional to the scaling of vdW radii, r_{vdW}. For example, recalculations using 0.9 and 1.1 times r_{vdW} lead to the linear EED changes. These tendencies reflect the exponent ζ for the spatial tails of MOs. The EEDs distribute exponentially from each atomic center around the vdW surfaces without showing irregular change. Therefore, the EED dependences are so monotonic that the propensities of EED distributions are retained well upon different definitions of Ω.

3.3. Interaction Potentials with He*. It is extremely time-consuming to perform ab initio calculations to evaluate the interaction potential energy between the highly excited He*(2^3S) and glycine conformers embedded in the ionization continuum. We employed a model potential, in which the He*(2^3S) atom is replaced by the Li atom. This approximation stems from the similarity between Li(2^2S) and He*(2^3S) in terms of the same outer valence. The fundamental nature of anisotropic interaction has been predicted successfully for many molecules.[45] Nonetheless, the differences in IEs (Li, 5.392 eV; He*, 4.768 eV) and 2s−2p energy gaps (Li, 1.848 eV; He*, 1.114 eV) would result in smaller electron-accepting and less polarizable character for the Li atom, respectively. For instance, the attractive well depths with alkali or rare-gas atoms are different by about 20%.[48] Any such deviation can, in principle, be corrected additively by adjusting the potential parameters to experimental CEDPICS.[45]

In this paper, we focus on the nature of conformational changes in anisotropic interactions for multidimensional accesses using this simple model. The interaction potential V_0 was thus obtained as

$$V_0 = E_{\mathrm{MLi}} - (E_{\mathrm{M}} + E_{\mathrm{Li}}) \quad (6)$$

where E_{MLi}, E_{M}, and E_{Li} are the energies of the interacting system M + Li, isolated molecule M, and isolated Li atom, respectively. $V_0(r)$ in various directions was calculated using the second-order Møller−Plesset perturbation theory (MP2) with 6-311++G(d,p) basis sets. The basis set superposition error was corrected by the full counterpoise method.[49] The structures of the molecules were fixed at the optimized geometries, and flexible motion over the shallow PES was not taken into account. The resultant V_0 potentials are the first examples of the interaction potential of amino acids with He*.

4. Results and Discussion

4.1. Conformational Isomers. The calculated lowest five conformers of glycine are depicted in Figure 1 with notations used by Császár.[17] The conformational stability is determined by a balance between the attractive hydrogen-bonding interaction and the repulsive bond−bond interaction. The competitive forces lead to equilibrium structures with slightly staggered conformations belonging to the C_1 point group and eclipsed ones in the C_s symmetry in a close energy range. These two forms are denoted by n or p in Figure 1, respectively.

The relative electronic energies ΔU and zero-point-energy (ZPE)-corrected ones are given in Table 1. The calculated order of electronic energy ΔU is in line with that of previous calculations using smaller basis sets aug-cc-pVDZ,[11] 6-311G(d,p),[24] and 6-311++G(d,p)[17,50] at the B3LYP or MP2 levels. However, the torsional stabilities between the p and n forms were found to be fairly basis set dependent. The differences of ΔU are calculated to be significantly small for conformers II and III, being 0.03 and 0.02 kJ mol^{-1}, respectively, at B3LYP/aug-cc-pVTZ. Therefore, vibrational effects from ZPEs are far greater than the energy differences. It is also noted that the statistical effects of entropy contribute to the total energy at finite temperatures.[50] The nonelectronic contributions are likely to play a crucial role in conformational dynamics and fluctuations because the low-frequency vibrational levels on the shallow potentials are significantly populated.

The conformational stability of I−IV (we omit p and n hereafter) relates to the strength of intramolecular hydrogen bonding. The calculated geometrical parameters show that hydrogen bonds are formed in I−III along the central bond (Table S1 in the Supporting Information). Given that the repulsive bond−bond interactions are similar, the relative energies ΔU in the order I → II → III suggest stronger hydrogen bonds at O5(carbonyl) → N3 → O4(hydroxyl). The fact that III is less stable than IV supports this tendency and is ascribed to the gauchelike conformation of IV ($\tau_{3215} = -17.4°$). The two types of possible hydrogen bonding at carbonyl and hydroxyl O atoms make the conformational rotation easy between I and III, whereas the hydrogen bonds at the N atom in II do not have such counterparts. Consequently, the isomerization barriers separating I−II and II−III (∼80 kJ mol^{-1})[7] are significantly greater than that of I−III (∼3 kJ mol^{-1}).[7,50]

4.2. UPS and Conformational Distribution. Figure 2 presents observed and calculated He I UPS of glycine. The observed He I UPS is similar to the previously reported He II UPS.[28] The only difference is that the latter contains C_{2s} bands. The calculated spectra shown at the bottom were synthesized from the calculated adiabatic IEs and pole strengths from the OVGF/cc-pVTZ calculations. Gaussian distributions with fwhm of 0.5 eV were convoluted without any empirical adjustment. Here, we sum up each spectrum of conformers I−IV with statistical weights. The statistical ratio is adopted from a theoretical study[50] that includes quantum effects such as ZPE. The ratio employed was I (71%), II (10%), III (8%), IV (9%), and V (2%) at 260 °C, respectively.

The summed theoretical UPS spectrum qualitatively agrees with the transmission-corrected experimental UPS spectrum in Figure 2. The positions of the higher bands 1−4 are well reproduced. Discrepancy is seen between separately observed bands 5 and 6 and overlapped calculated bands 5 and 6. The disagreement is ascribed to the too closely calculated IEs for bands 5 and 6 shown in Table 2 because the observed PIES spectra shown in Figure 3 also display separate bands 5 and 6 in contrast to the calculation. Changing the partitioning ratio, such as that for II, would not lead to a better agreement with the observed UPS spectrum. The calculated pole strengths exceeding 0.9 support the orbital picture for all of the conform-

TABLE 3: Calculated IEs (eV) and EEDs for Glycine Conformers II−V

conformer	MO	OVGF cc-pVTZ[b]	OVGF TZVP[c]	P3 6-311+G(d,p)[e]	EED[f] (%)
II (C_s)	16a′ ($n_{O//}$)	10.16 (0.91)	10.0		3.13
	15a′ (n_N)	11.57 (0.91)	11.7[d]		3.34*
	4a″ ($n_{O\perp}$)	11.60 (0.90)	11.5[d]		2.76
	14a′ ($n_{O//}$)	13.66 (0.91)	13.9[d]		1.74
	3a″ (π_{CH_2})	13.88 (0.91)	13.7[d]		2.62
	13a′ (σ_{CO})	15.25 (0.91)	15.4		1.81
	2a″ (π_{OCO})	15.51 (0.90)	15.8		2.64
	12a′ (σ_{CN})	16.66 (0.90)	16.7		1.51
	11a′ ($n_{O//}$)	17.91 (0.90)	18.8[d]		1.73*
	1a″ (π_{NH_2})	18.33 (0.91)	18.0[d]		2.68
III (C_s)	16a′ (n_N)	9.74 (0.91)	9.7	9.6	3.92
	15a′ ($n_{O//}$)	11.78 (0.91)	12.3[d]	11.4	3.09
	4a″ ($n_{O\perp}$)	12.15 (0.90)	11.9[d]	12.0	2.56
	3a″ (π_{CH_2})	13.76 (0.92)	13.7	13.6	2.84
	14a′ (σ_{CN})	14.55 (0.91)	14.6	14.5	2.35
	13a″ ($n_{O//}$)	14.79 (0.91)	14.9	14.6	1.62
	2a″ (π_{OCO})	15.59 (0.90)	15.8		2.47
	12a′ (σ_{CO})	17.01 (0.90)	17.3		1.38
	11a′ ($n_{O//}$)	17.25 (0.91)	17.8[d]		1.52*
	1a″ (π_{NH_2})	17.67 (0.91)	17.6[d]		2.83
IV (C_1)	20a′ (n_N)	9.88 (0.91)			4.90
	19a′ ($n_{O//}$)	11.16 (0.91)			2.47
	18a′ ($n_{O\perp}$)	12.29 (0.90)			2.77
	17a′ (σ_{CC})[a]	14.11 (0.92)			2.17
	16a′ (π_{CH_2})[a]	14.36 (0.91)			1.91
	15a′ (π_{CN})[a]	14.94 (0.91)			2.30
	14a′ (σ_{NH_2})[a]	15.65 (0.91)			2.02
	13a′ (π_{OCO})[a]	16.72 (0.90)			3.01
	12a′ ($n_{O//}$)	17.30 (0.91)			1.65
	11a′ (σ_{CO})[a]	17.88 (0.90)			1.61
V (C_1)	20a′ (n_N)	9.91 (0.91)			4.66
	19a′ ($n_{O//}$)	11.15 (0.91)			2.78
	18a′ ($n_{O\perp}$)	12.24 (0.90)			2.84
	17a′ (σ_{CH})[a]	14.02 (0.92)			2.32
	16a′ ($n_{O//}$)	14.44 (0.91)			1.83
	15a′ (σ_{CN})[a]	14.82 (0.91)			2.46
	14a′ (σ_{NH_2})[a]	16.21 (0.91)			1.87
	13a′ (σ_{CH})[a]	16.70 (0.90)			2.84
	12a′ (σ_{CO})[a]	16.98 (0.90)			1.57
	11a′ ($n_{O//}$)	17.49 (0.91)			1.66

[a] Approximate descriptions because these conformers possess no symmetry planes. [b] Pole strengths are in parentheses. [c] Reference 25. [d] The orders of these bands are reversed. [e] Reference 24. [f] EEDs calculated at SCF/6-311++G(d,p). Asterisks indicate those involved in hydrogen bonding.

ers. The unresolved vibrational progressions are possibly due to by the overlapping of each spectrum. Bands 4−10 are observed more strongly in the present He I UPS spectrum than in the previous He II UPS spectrum.[28] The calculated weakness of bands 4−10 of the UPS spectrum in Figure 2 and the PIES spectrum in Figure 3 implies the presence of an overlapped background below an electron energy of less than ∼8 eV. Otherwise, the transmission efficiency of the analyzer is likely to be responsible for it.

4.3. PIES and Spectral Assignments. Figure 3 shows the PIES spectrum of glycine, which was recorded under collision energy 90−300 meV. The final theoretical PIES I + II + III + IV spectrum was obtained by summing up the spectra of each conformer. The good agreement with experiment demonstrates the applicability of the EED model in Figure 3, in which the prominent band 1 and weak bands 2 and 4 are qualitatively reproduced. The PIES spectrum is, in general, complementary to the UPS spectrum. The cross sections for PIES are fairly dependent upon the MOs to be ionized, as can be seen in Figure 3, whereas those for UPS are fairly similar (see Figure 2). These propensities give rise to the marked differences for bands 1−3 in the UPS and PIES spectra. Also, the strong PIES intensity of band 10 shifts the composite PIES bands 8−10 rightward.

The qualitative reproduction of PIES indicates a dominant role of EEDs. Tables 2 and 3 compile the calculated IEs and

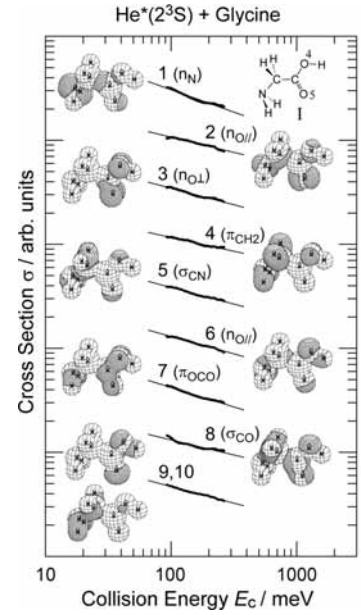

Figure 4. Collision energy dependence of partial ionization cross-sections for glycine with He*(2^3S), and corresponding molecular orbitals of glycine conformers I (71%) which are obtained from self-consistent-field (SCF) calculations using cc-pVTZ basis sets. Bold lines depict surfaces at which $|\phi_i|^2 = 10^{-4}$ Å^{-3} and thin lines represent van der Waals surfaces.

EEDs for conformers I−V, respectively, along with the experimental results of UPS and PIES. In these calculations, the geometrical parameters were set as those at the MP2/6-311++G(d,p) level. The largest EED value for band 1 in Table 2 indicates an important role of the nonbonding orbital (n_N) of the N atom. Peak energy shifts ΔE given in Table 2 are measured with respect to the "nominal" IE E, where E is the difference between the metastable excitation energy and target IEs. ΔE reflects the interaction energy between He* and the target molecule.[51] The ΔE values of band 1 (n_N) were found to be significantly negative, −0.33 eV, whereas that of band 3 ($n_{O\perp}$) is negligible. This tendency suggests the presence of an attractive interaction in the direction of n_N and a less attractive interaction in the out-of-plane direction. Also, ΔE of band 7 (π_{OCO}) is not as negative as −0.3 eV, in line with the fact that π_{OCO} extends in the out-of-plane direction. Collisional dynamics involving these repulsive or attractive interactions will be discussed in section 4.4.

As annotated in Tables 2 and 3, the present OVGF/cc-pVTZ calculations give different orders of IEs from the previous OVGF/TZVP calculations[25] in better agreement with the experiment. The deep bands of 8−10 are assigned differently to σ_{CO}, $n_{O//}$, and π_{NH_2} of conformer I, respectively.[25,28] If we assume that conformer I is dominating the observed spectra, the root mean squares are estimated to be 0.21 and 0.31 eV for the present and previous calculations, respectively. Comparisons of the calculated EEDs between conformers I−V lead to a general propensity: when the N and O atoms form hydrogen bonds, the nonbonding n_N and n_O orbitals distribute inside the molecular surface. Otherwise, the nonbonding orbitals display much larger EEDs. For example, the EED of n_N orbital in II is exceptionally small among the hydrogen-bond-related EEDs, which are asterisked in Tables 2 and 3.

4.4. Collision Energy Dependence. The partial cross section for Penning ionization to produce M_i^+ depends upon not only MO ϕ_i but also branching ratios. Namely, the trajectories of He* affect the ionization process and impose additional effects

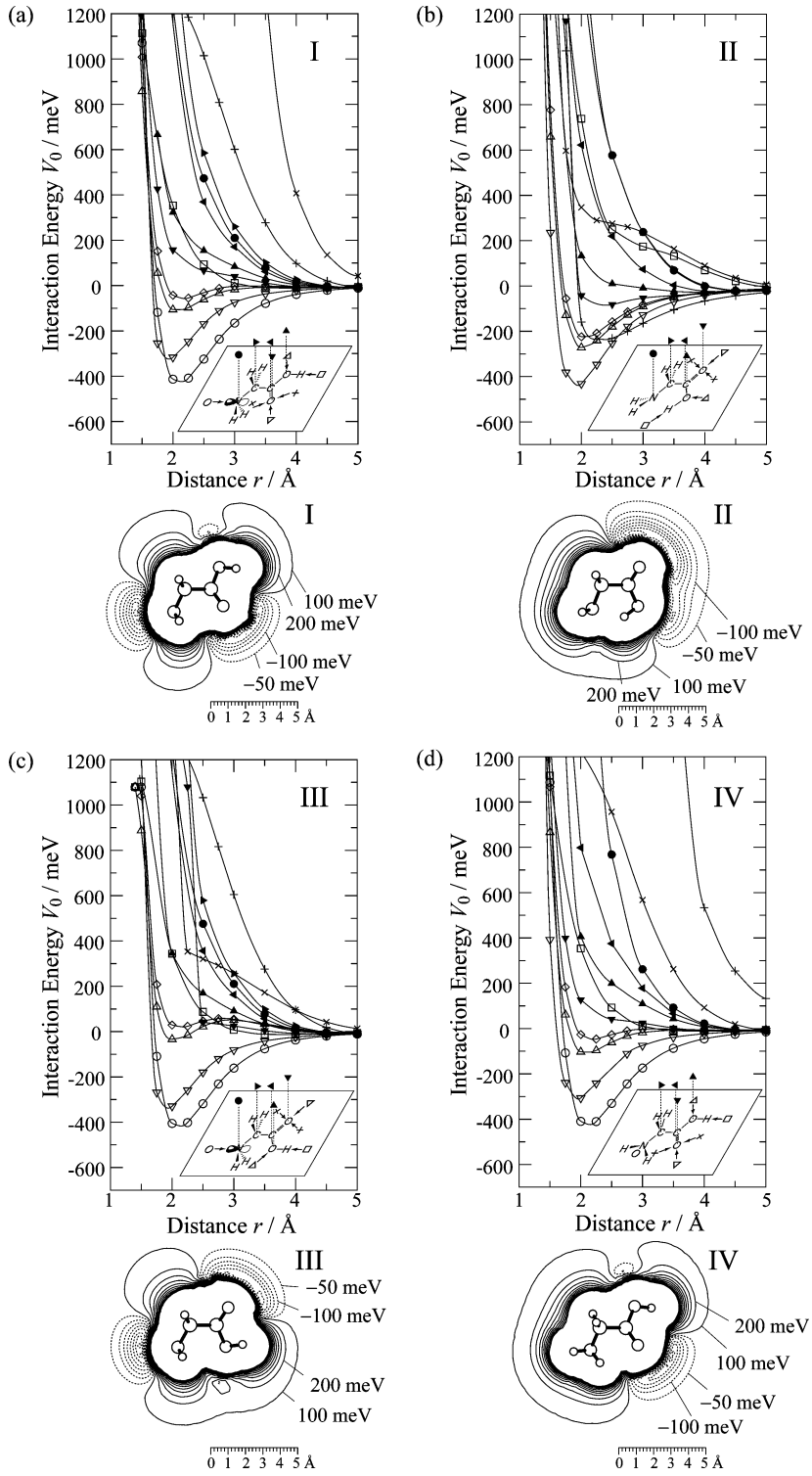

Figure 5. (Upper) Interaction potential energy curves of V_0 as a function of the distance r between a targeted atom and Li(He*) in different directions of approach of the colliding Li(He*). Legend: (○) averaged direction of the three bonds stemming from the N atom; (△) direction bisecting the two bonds of the O atom; (▽) along the C═O bond; (× and +) perpendicular to the C═O bond; (right-pointing ▲, left-pointing ▲, ▼, ●) out-of-plane directions with respect to the plane defined by framework NCCOO. (Lower) Contour maps of the in-plane V_0. The energy spacing of contour lines is set as 100 meV for positive values and 50 meV for negative values.

on the EED approximation. The trajectories are determined by the relative velocity and interaction potentials around the molecule. Thus, we discuss ionization dynamics with respect to collision energy dependence and interaction potentials.

Figure 4 shows collision energy (E_c) dependences of partial ionization cross sections (σ_i) (CEDPICS) as log σ_i vs log E_c plots in arbitrary units. It also visualizes the MOs ϕ_i as three-dimensional contour surfaces. The bold lines depict contour surfaces at which $|\phi_i|^2 = 10^{-4}$ Å^{-1}, whereas the thin lines represent vdW spheres. The CEDPICS are fit by linear regression analyses, and slopes m are given in Table 2. The collision energy dependences are explained satisfactorily, assuming dominant conformer I.

The most inclined CEDPICS is obtained for band 1 with $m = -0.42$. It is well-known that the negative slope ($m < 0$) is related to an attractive potential well in atom−atom systems.[51−53]

If the long-range attractive part of interaction potential $V^*(r) \propto r^{-s}$ plays a dominant role, $\sigma(E_c)$ is proportional to $E_c^{-2/s}$ and the slope $m = -2/s$ is negative. Therefore, the interaction in the direction of the n_N orbital is attractive, and the long-range dependence for band 1 is estimated to be $s = 4.8$. In this direction, only the n_N orbital shows a significant EED and other valence orbitals do not. Hence, the extended n_N lobe would most contribute to the electronic interaction with He*, and the attractive interaction relates to the orbital overlap between the extended N sp^3 lobe and the He* 2s orbital. For a more detailed understanding, we performed quantum chemical calculations in various directions.

4.5. Reaction Dynamics on PES. The interaction potential curves shown in the upper parts of Figure 5 are obtained from single-point-energy calculations at the MP2(full)/6-311++G(d,p) level for the various kinds of approaches of the colliding Li(2^2S). The distances r is measured from the targeted atom to the Li atom. On the other hand, the contour maps shown in the lower parts display two-dimensional anisotropies of interaction energy in the molecular plane spanned by the NCCOO frame. These are obtained from the interpolations of single-point energies calculated at the MP2/6-311++G(d,p) level employing the frozen-core approximation. In these calculations of the 2D interaction energy, the grid points are placed at intervals 0.5 Å in the radial direction from the center of mass and at azimuthal angle steps 7.5° in the molecular plane. The total number of grid points was ~960. The calculated energies are first interpolated in the radial directions with cubic-spline functions, and the resultant potential energy curves are connected in the azimuthal directions with other spline functions. Structural relaxation from the equilibrium structures was not taken into account.

Indeed, attractive potential curves are found for all of the conformers, as shown in Figure 5. Similar depths are obtained in the directions of n_N orbitals and C═O bonds, except when n_N are involved in hydrogen bonding. That is, the potential well are located around O atoms in conformer II, and access toward the N atom is shielded by substituent atoms. The present calculations demonstrate the remarkable attractive interaction at nonbonding orbital n_N. The fact that the directions of n_N orbitals (○) and C═O bonds (▽) are similarly attractive unless shielding effects of the substituents indicates similar tendencies between Li(He*) and hydrogen-bonding interactions. Most of the out-of-plane directions indicated with filled legends are calculated to be repulsive. These analyses qualitatively describe the entrance channel dynamics of the colliding system He* + glycine. The collision-induced conformational change upon collision with light He atoms has been found to be less probable in the present collision energy range. However, such changes are likely to be induced by heavier colliding atoms like Ne and Ar.[54]

These PESs are connected with the observed PIES intensities, peak shifts, and CEDPICS. First, the most significant discrepancy found between the experimental and theoretical PIES intensities for band 2 (π_{CH_2}) can be explained by the deep attractive potential well around the n_N orbital of conformer I. The reaction probabilities predicted by EEDs are disturbed by the branching of He* approach toward such attractive regions. In contrast, the CH_2 region where the π_{CH_2} orbital extends (Figure 4) is repulsive, and the He* access could be deflected away. Second, the significant negative peak shifts ΔE observed for bands 1 (n_N) and 5 (σ_{CN}) in Table 2 are also caused by the attractive interactions. Collisional ionization around the N atom and O atoms (Figure 4) are likely to be responsible for these negative ΔEs. Third, the negative CEDPICS and m values obviously indicate the presence of attractive interactions. The most negative dependence of band 1 is explained by the deepest potential well −422 meV in conformer I. If the repulsive part of the interaction potential $V^*(r)$ governs the collision energy dependence, the slope m becomes positive.[52] Hence, the reaction dynamics of this type could make the m parameter of band 4 less negative.

5. Conclusions

This paper has demonstrated collision-energy-resolved PIES on amino acids for the first time. The significantly large EEDs and attractive interaction with He* have been obtained for nonbonding n_N orbitals. In the most stable conformer of glycine, the hydrogen bonds involving the H atoms of the NH_2 group make the n_N orbital point outward. The extended n_N orbital gives rise to large Penning ionization cross sections, negative peak shifts, and negative collision energy dependences. The direction along C═O bonds has also been found to be attractive. These properties and spatial shielding effects to the orbitals around N and O atoms can be used as markers for the structures of hydrogen-bonding networks. The theoretical spectra on the basis of OVGF and EED calculations have qualitatively reproduced the observed PIES. The exceptional disagreement found for the π_{CH_2} band is likely due to reaction branching affected by the attractive/repulsive interactions.

Acknowledgment. This work was supported by a Grant-in-Aid for Scientific Research (C) (Grant 19550002, 2007) from the Japan Society for the Promotion of Science. The authors acknowledge Dr. Masayo Yamauchi for her participation at the early stage of this work.

Supporting Information Available: Electron density contours for conformers II−V and optimized geometrical parameters. This material is available free of charge via the Internet at http://pubs.acs.org.

References and Notes

(1) Locke, M. J.; MaIver, R. T., Jr. *J. Am. Chem. Soc.* **1983**, *105*, 4226.
(2) Brown, R. D.; Godfrey, P. D.; Storey, J. W. V.; Bassez, M.-P. *J. Chem. Soc., Chem. Commun.* **1972**, 547.
(3) Suenram, R. D.; Lovas, F. J. *J. Mol. Spectrosc.* **1978**, *72*, 372.
(4) Suenram, R. D.; Lovas, F. J. *J. Am. Chem. Soc.* **1980**, *102*, 7180.
(5) Brown, R. D.; Crofts, J. G.; Godfrey, P. D.; McNaughton, D.; Pierlot, A. P. *J. Mol. Struct.* **1988**, *190*, 185.
(6) Godfrey, P. D.; Brown, R. D. *J. Am. Chem. Soc.* **1995**, *117*, 2019.
(7) Godfrey, P. D.; Brown, R. D.; Rodgers, F. M. *J. Mol. Struct.* **1996**, *376*, 65.
(8) Lovas, F. J.; Kawashima, Y.; Grabow, J.-U.; Suenram, R. D.; Fraser, G. T.; Hirota, E. *Astrophys. J.* **1995**, *455*, L201.
(9) Iijima, K.; Tanaka, K.; Onuma, S. *J. Mol. Struct.* **1991**, *246*, 257.
(10) Reva, I. D.; Plokhotnichenko, A. M.; Stepanian, S. G.; Ivanov, A. Y.; Radchenko, E. D.; Sheina, G. G.; Blagoi, Y. P. *Chem. Phys. Lett.* **1995**, *232*, 141.
(11) Stepanian, S. G.; Reva, I. D.; Radchenko, E. D.; Rosado, M. T. S.; Duarte, M. L. T. S.; Fausto, R.; Adamowicz, L. *J. Phys. Chem. A* **1998**, *102*, 1041.
(12) Huisken, F.; Werhahn, O.; Ivanov, A. Y.; Krasnokutski, S. A. *J. Chem. Phys.* **1999**, *111*, 2978.
(13) Vishveshwara, S.; Pople, J. A. *J. Am. Chem. Soc.* **1977**, *98*, 2422.
(14) Schäfer, L.; Sellers, H. L.; Lovas, F. J.; Suenram, R. D. *J. Am. Chem. Soc.* **1977**, *98*, 2422.
(15) Jensen, J. H.; Gordon, M. S. *J. Am. Chem. Soc.* **1991**, *113*, 7917.
(16) Frey, R. F.; Coffin, J.; Newton, S. Q.; Ramek, M.; Cheng, V. K.; Momany, F. A.; Shafer, L. *J. Am. Chem. Soc.* **1992**, *114*, 5369.
(17) Császár, A. G. *J. Am. Chem. Soc.* **1992**, *114*, 9568.
(18) Hu, C. H.; Shen, M.; Schaefer, H. F., III. *J. Am. Chem. Soc.* **1993**, *115*, 2923.
(19) Császár, A. G. *J. Mol. Struct.* **1995**, *346*, 141.
(20) Zheng, Y.; Neville, J. J.; Brion, C. E. *Science* **1992**, *270*, 786.

(21) Barone, V.; Adamo, C.; Lelj, F. *J. Chem. Phys.* **1995**, *102*, 364.
(22) Neville, J. J.; Zheng, Y.; Brion, C. E. *J. Am. Chem. Soc.* **1996**, *118*, 10533.
(23) Nguyen, D. T.; Scheiner, A. C.; Andzelm, J. W.; Sirois, S.; Salahub, D. R.; Hagler, A. T. *J. Comput. Chem.* **1997**, *13*, 1609.
(24) Herrera, B.; Dolgounitcheva, O.; Zakrzewski, V. G.; Toro-Labbé, A.; Ortiz, J. V. *J. Phys. Chem. A* **2004**, *108*, 11703.
(25) Falzon, C. T.; Wang, F. *J. Chem. Phys.* **2005**, *123*, 214307.
(26) Debies, T. H.; Rabalais, J. W. *J. Electron Spectrosc. Relat. Phenom.* **1974**, *3*, 315.
(27) Cannington, P. H.; Ham, N. S. *J. Electron Spectrosc. Relat. Phenom.* **1979**, *15*, 79.
(28) Cannington, P. H.; Ham, N. S. *J. Electron Spectrosc. Relat. Phenom.* **1983**, *32*, 139.
(29) Richer, G.; Sandorfy, C.; Mascimento, M. A. C. *J. Electron Spectrosc. Relat. Phenom.* **1984**, *34*, 327.
(30) Penning, F. M. *Naturwissenschaften* **1927**, *15*, 818.
(31) Niehaus, A. *Adv. Chem. Phys.* **1981**, *45*, 399.
(32) Hotop, H.; Niehaus, A. *Z. Phys.* **1969**, *228*, 68.
(33) Yamakita, Y.; Tanaka, H.; Maruyama, R.; Yamakado, H.; Misaizu, F.; Ohno, K. *Rev. Sci. Instrum.* **2000**, *71*, 3042.
(34) Ohno, K.; Yamakado, H.; Ogawa, T.; Yamata, T. *J. Chem. Phys.* **1996**, *105*, 7536.
(35) Kishimoto, N.; Aizawa, J.; Yamakado, H.; Ohno, K. *J. Phys. Chem. A* **1997**, *101*, 5038.
(36) Gardner, J. L.; Samson, J. A. R. *J. Electron Spectrosc. Relat. Phenom.* **1976**, *8*, 469.
(37) Kimura, K.; Katsumata, S.; Achiba, Y.; Yamazaki, T.; Iwata, S. *Handbook of He I Photoelectron Spectra of Fundamental Organic Molecules*; Japan Scientific: Tokyo, 1981.
(38) *Atomic and Molecular Beam Methods*; Scoles, G., Ed.; Oxford University Press: New York, 1988; Vol. 1.
(39) Becke, A. D. *J. Chem. Phys.* **1993**, *98*, 5648.
(40) Lee, C.; Yang, W.; Parr, R. G. *Phys. Rev. B* **1988**, *37*, 785.
(41) Dunning, T. H., Jr. *J. Chem. Phys.* **1989**, *90*, 1007.
(42) Kendall, R. A.; Dunning, T. H., Jr. *J. Chem. Phys.* **1992**, *96*, 6796.
(43) Frisch, M. J.; Trucks, G. W.; Schlegel, H. B.; Scuseria, G. E.; Robb, M. A.; Cheeseman, J. R.; Montgomeri, J. A., Jr.; Vreven, T.; Kudin, K. N.; Burant, J. C.; Millam, J. M.; Iyengar, S. S.; Tomasi, J.; Barone, V.; Mennucci, B.; Cosi, M.; Scalmani, G.; Rega, N.; Petersson, G. A.; Nakatsuji, H.; Hada, M.; Ehara, M.; Toyota, K.; Fukuda, R.; Hasegawa, J.; Ishida, M.; Nkajima, T.; Honda, Y.; Kitano, O.; Nakai, H.; Klene, M.; Li, X.; Knox, J. E.; Hratchian, H. P.; Cross, J. B.; Adamo, C.; Jaramillo, J.; Gomperts, R.; Stratmann, R. E.; Yazyev, O.; Austin, A. J.; Cammi, R.; Pomelli, C.; Ochterski, J. W.; Ayala, P. Y.; Morokuma, K.; Voth, G. A.; Salvador, P.; Dannenberg, J. J.; Zakrzewski, V. G.; Dapprich, S.; Daniels, A. D.; Strain, M. C.; Farkas, O.; Malick, D. K.; Rabuck, A. D.; Raghavachari, K.; Foresman, J. B.; Ortiz, J. V.; Cui, Q.; Baboul, A. G.; Clifford, S.; Cioslowski, J.; Stefanov, B. B.; Liu, G.; Liashenko, A.; Piskorz, P.; Komaromi, I.; Martin, R. L.; Fox, D. L.; Keith, T.; Al-Laham, M. A.; Peng, C. Y.; Nanayakkara, A.; Challacome, M.; Gill, P. M. W.; Johnson, B.; Chen, W.; Wong, M. W.; Conzalez, C.: Polple, J. A. *Gaussian 03*, revision D.01; Gaussian, Inc.: Wallingford, CT, 2004.
(44) Ohno, K.; Mutoh, H.; Harada, Y. *J. Am. Chem. Soc.* **1983**, *105*, 4555.
(45) Ohno, K. *Bull. Chem. Soc. Jpn.* **2004**, *77*, 887.
(46) Bondi, A. *J. Phys. Chem.* **1964**, *68*, 441.
(47) For example: Yamakita, Y.; Yamauchi, M.; Ohno, K. *Chem. Phys. Lett.* **2000**, *322*, 189.
(48) Hotop, H.; Roth, T. E.; Ruf, M.-W.; Yencha, A. J. *Theor. Chem. Acc.* **1998**, *100*, 36.
(49) Boys, S. F.; Bernardi, F. *Mol. Phys.* **1970**, *19*, 553.
(50) Miller, T. F., III; Clary, D. C. *Phys. Chem. Chem. Phys.* **2004**, *6*, 2563.
(51) Čermak, V. *J. Chem. Phys.* **1966**, *44*, 3781.
(52) Illenberger, E.; Niehaus, A. *Z. Phys. B* **1975**, *20*, 33.
(53) Allison, W.; Muschlitz, E. E., Jr. *J. Electron Spectrosc. Relat. Phenom.* **1981**, *23*, 339.
(54) Miller, T. F., III; Clary, D. C.; Meijer, A. J. H. M. *J. Chem. Phys.* **2005**, *122*, 244323.

JP9038978